POAC'23
Glasgow, United Kingdom

Proceedings of the 27th International Conference on
Port and Ocean Engineering under Arctic Conditions
12-16 June 2023, Glasgow, United Kingdom

Measurements of surface waves propagating cross the ice edge in Spitsbergen fjord

Aleksey Marchenko[1], Nataly Marchenko[1], Rocky Taylor[2]
[1] The University Centre in Svalbard, Longyearbyen, Norway
[2] Memorial University if Newfoundland, St. Johns, Canada

ABSTRACT

Field measurements of sea water and ice properties were performed the Raudfjorden on the North of Spitsbergen on March 8-9, 2022. The temperature, salinity, density, speed of p-waves, elastic moduli, and flexural strength of the ice were measured. Thin section analysis demonstrated granular structure of the ice. To record wave characteristics, we deployed temperature and pressure recorders SBE-39Plus at different depths, acoustic doppler velocimeter, and the IMU buoy on the ice. The data collected with these sensors provided the information on wave characteristics in specific points where the sensors were deployed. In addition, we used laser scanning with Riegl Vz-1000 to get the spatial shape of sea ice deformed by waves. Results of the measurements are discussed in the paper.

KEY WORDS: Sea ice; Heat flux; Elastic modulus; Flexural strength; Waves.

1. INTRODUCTION

Climate change influences local weather conditions and ice formation in the Arctic. Fast changes of air temperature from positive to relatively low values below -20 C influence sea ice formation in limited and relatively short time periods with duration of 1-2 weeks. Between these periods the air temperature varies near the freezing point and ice thickness doesn't increase or even decreases under the action of ocean heat flux. The equilibrium ice thickness is determined by the balance of the heat flux from the ocean and cold flux from the air. In such conditions relatively stable sea ice forms in Spitsbergen fjords and don't form in open sea.

Blue line in Fig. 1 shows the mean air daily temperature recorded on the weather station in New-Alesund from October 1, 1982, to June 1, 1983. Yellow and green lines in Fig. 1 shows

respectively the mean air daily temperature recorded on the weather stations in New-Alesund and Verlegenhuken from October 1, 2021, to June 1, 2022. Locations of the weather stations are pointed out in Fig. 2a by blue squares NA and V. We assume that the air temperature in the Raudfjorden located on the northern coast of Spitsbergen to the West from Verlegenhuken was similar the temperatures shown in Fig. 1. Eight months with negative air temperatures influence formation of sea ice in the fjord.

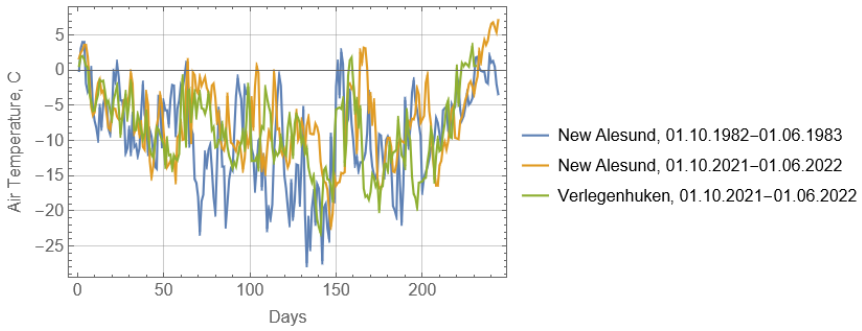

Figure 1. Air temperatures recorded on weather stations in New-Alesund (pink line) and Verlegenhuken (aquamarine line) from October 1 to June 1 in 1980 and 2022.

Sea ice is an important component of northern nature influencing energy exchange between atmosphere and ocean. Sea ice properties are important for the safety transport communications and tourism. Sea ice is important component of biological systems of polar regions. Life cycle of seals and polar bears depend on the duration of ice season. Actions of wind and waves may destroy sea ice on big areas of open sea in a short time. In the fjords sea ice is more stable but also subjected by natural actions. In the present paper we describe properties of sea ice in the Raudfjorden on the North of Spitsbergen based on the results of field works in March 2022 and compare it with the ice properties investigated in the same place in 1983 (Squire, 1984).

2. FIELD WORKS

The field works were performed during the cruise of Polarsyssel on March 8-9, 2022. The track of Polarsyssel is shown in Fig. 2a. Locations of the field works near the ice edge (IE) in the open sea (OS) are pointed out by orange circles. Ice conditions are shown on the ice chart in Fig. 2a. Observation from the shipboard showed that sea was free from the ice to the North of Spitsbergen, while thin continuous ice was observed in the fjords of northern Spitsbergen. This ice is shown by grey and red colours in Fig. 2b.

Polarsyssel approached the ice edge in the Raudfjorden on March 8. Drilling near the ice edge showed the ice thickness of around 20 cm. The field works on the floating ice were performed on March 8 and March 9 near the board of Polarsyssle. For the night time on March 8-9 the ship left ice edge and was standing in the open sea. Figure 3a shows the schematic of equipment deployed on sea ice near the ice edge. Ice tracker (IT) equipped with IMU (Oceanetic Measurements LtD) was mounted on 25 m distance from the ice edge on March 8. It recorded 3 accelerations, 3 angles of rotation of the buoy, and magnetic

inclination angles. The Acoustic Doppler Velocimeter (ADV in Fig. 3a, Sontek Ocean Probe 5 MHz) was installed in downlooking position together with pressure and temperature recorded SBE 39Plus (SBE1 in Fig. 3a) on 10 m distance from the ice edge on March 9. SBE1 recorded water temperature at 45 cm depth below the water level. The sampling rate and burst length were programmed respectively to 10 Hz and 1200 s. The ADV was powered from the ship. Deployment locations of IT and ADV are shown in Fig. 3b.

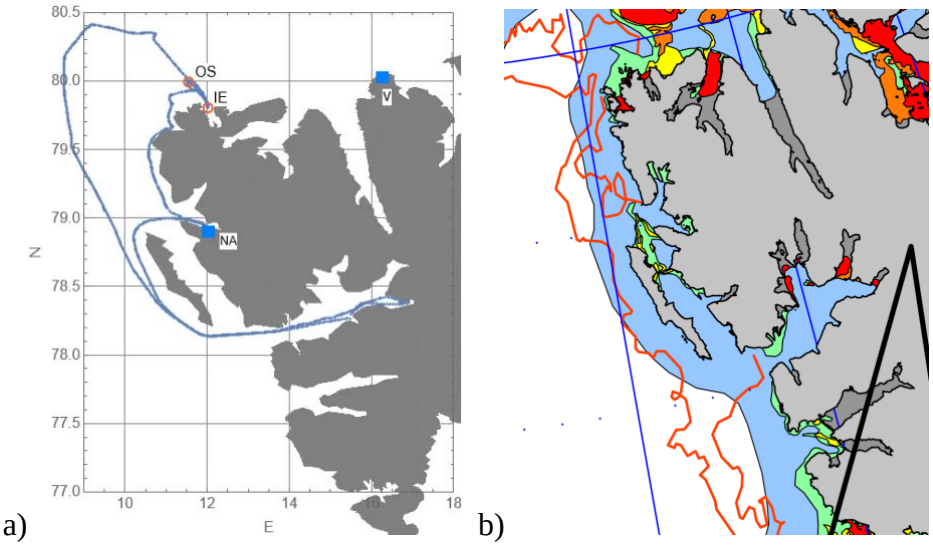

a) b)

Figure 2. (a) Polarsyssel track on March 7-12, 2022. (b) Ice conditions on March 9, 2022 (http://polarview.met.no).

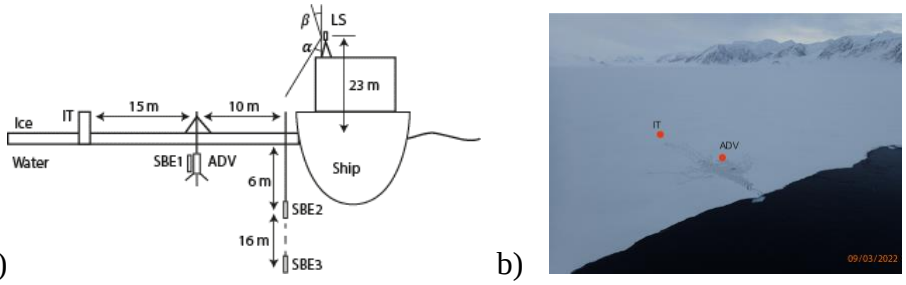

a) b)

Figure 3. (a) Schematic of equipment deployment during the field works on March 8-9, 2022. (b) Ice edge in the Raudfjorden. Locations of IT and ADV deployments are pointed out.

Two temperature and pressure recorders SBE 39Plus (SBE2 and SBE3 in Fig. 3a) were fixed on a rope and deployed on the depths 6 m and 16 m. The rope was mounted on the shipboard. The pressure records were used to calculate water surface elevation caused by waves near the ship (Marchenko, 2018). The pressure records were performed in locations OS and IE (Fig. 2a). Measurments of the vertical profiles of sea water temperature and salinity were performed in locations OS and IE up to 70 m depth with CTD recorder SBE 19.

The shape of ice surface near the ice edge was investigated by laser scanning with terrestrial scanner Riegle Vz-1000. The scanner was mounted on the ship desk oat 23 m height above sea ice surface (Fig. 3a). Each scan is performed on 360o in the horizontal plane and on 130^o in the vertical plane within the angle shown in Fig. 3 with α=30^o and β=20^o. The time of full

scan was programmed to 13 min. The full scan included scans in vertical direction over each 0.04º. Therefore, the full scan included 9000 vertical scans in different horizontal directions, and the time of each vertical scan was 0.086 s. This time is much smaller periods of swell (~10 s) and ship oscillation (pitch, roll, and heave). This circumstance allows to get ice shape deformed by waves in different spatial directions.

3. RESULTS OF FIELD MEASUREMENTS

Data of ADV and SBE

Figure 5a shows the spectrum of vertical accelerations recorded by IT from March 8, 15.00 UTC to March 9, 09.00. It includes local maxima around the frequencies 0.1 Hz, 0.155 Hz, and 0.35 Hz. Figure 5b shows the spectrum of the difference of water pressure fluctuations Δp is determined by the formula $\Delta p = p_6 - \langle p_6 \rangle - p_{16} + \langle p_{16} \rangle$, where p_6 and p_{16} are water pressures recorded at 6 m and 16 m depths, and $\langle p_6 \rangle$ and $\langle p_{16} \rangle$ are the mean values of the pressures. The data were recorded recorders from March 8, 19.00 to March 9, 07.00. The influence of ship oscillations is not included in the pressure Δp since both sensors SBE2 and SBE3 are mounted on the same rope. Spectral maxima at 0.1 Hz and 0.155 Hz are visible in the spectrum.

Figure 6a shows the spectrum of vertical accelerations recorded by IT from March 9 from 9.15 to 12.05 (blue line) and from 12.05 to 15.15 (yellow line). Blue line indicates the spectral maxima around 0.1 Hz, 0.155 Hz, 0.25 Hz and 0.4 Hz. Yellow line indicates decreasing energy of high harmonics with the frequencies 0.155 Hz, 0.25 Hz and 0.4 Hz after 12.00, March 9. The velocity spectrums in Fig. 6b also indicate in this time waves with the frequency of around 0.1 Hz.

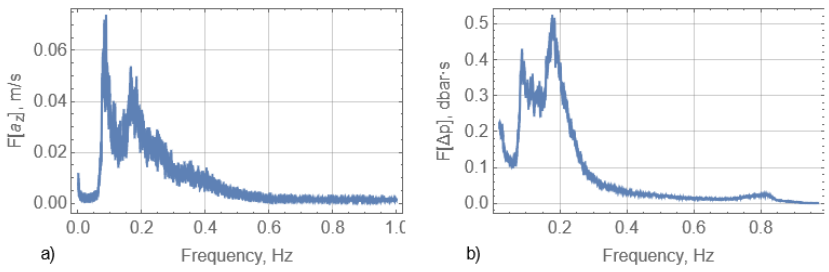

Figure 5. Spectrums of the vertical acceleration measured by IT from March 8, 15.00 UTC to March 9, 09.00 (a) and water pressure Δp (b) measured respectively the pressure recorders from March 8, 19.00 to March 9, 07.00 UTC (blue line).

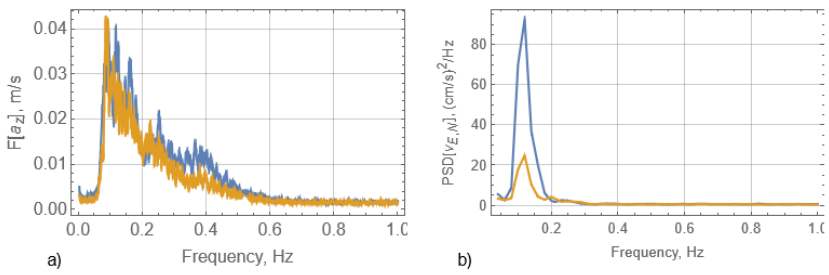

Figure 6. (a) Spectrums of the vertical accelerations recorded by IT on March 9 from 9.15 to 12.05 (blue line) and from 12.05 to 15.15 (yellow line). (b) Spectrums of East (blue line) and North (yellow line) water velocities recorded by ADV on March 9 from 15.00 to 16.00. UTC time is used.

Short term measurements of vertical accelerations of sea ice surface were performed with the uniaxial accelerometer Bruel & Kjær DeltaTron Type 8344 designed for the measurements of vibrations in the frequency range from 0.2 Hz to 3 kHz. The sampling frequency of the accelerometer was programmed to 20 kHz. The example of the record on 9.40 UTC, March 9, is shown in Fig. 7a. Oscillations with period 2-4 s are visible. It corresponds to the spectral maxima near 0.4 Hz on the blue line in Fig. 6a.

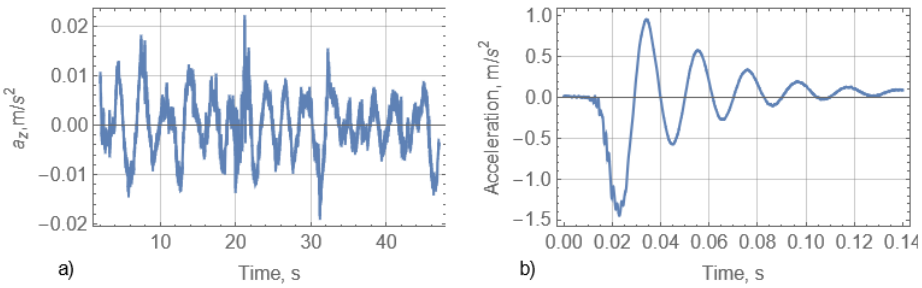

Figure 7. Vertical accelerations of ice surface recorded on March 9 at 9.46 UTC (a). Vertical acceleration recorded in the middle of fixed ends beam (b).

Data of laser scanning

Laser scanner data were analysed along 5 beams shown in Fig. 7. The scanning started at 15.30 UTC and extended for 13 min. The shapes of sea ice surface are shown in Fig. 9 for each direction. Two wavelengths of around 150 m are well visible along beam 1 in Fig. 9. Wave attenuation is not visible. Sea ice profiles along the other beams don't show perfect wavelengths, but also don't demonstrate attenuation of wave amplitude.

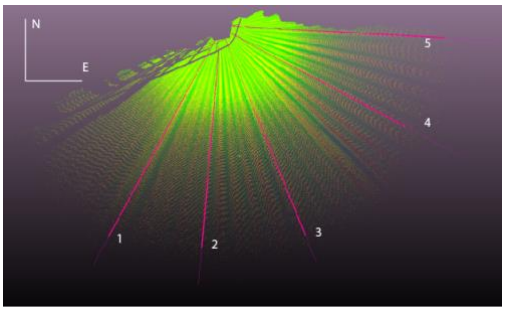

Figure 8. Directions of laser scanner beams 1-5 at 15.30 UTC, March 9.

Assuming small influence of ice on waves with 150 m wavelength we estimate the wave frequency ω from the dispersion equation of surface gravity waves on deep water $\omega^2=gk$, where k is the wave number. Assuming $k=2\pi/150$ m^{-1} we find $\omega=0.64$ rad/s (0.1 Hz). It corresponds well the spectrums shown in Fig. 6.

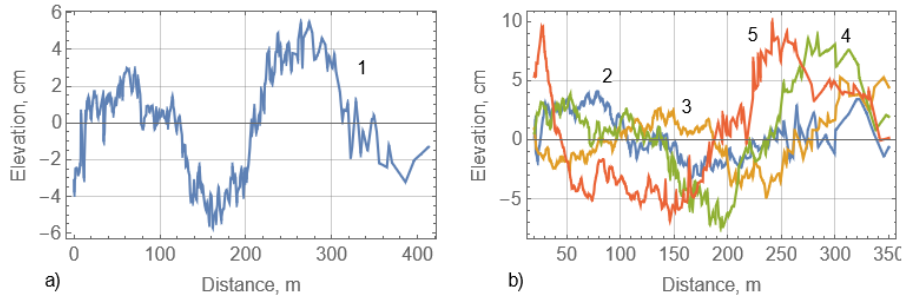

Figure 9. Ice surface shapes along laser beams 1-5.

Temperature and salinity profiles and heat fluxes

Temperature and salinity profiles measured over 70 m depth are shown in Fig. 10. One can see that sea water is warmer and saltier in the open sea than near the ice edge. In both locations the water temperature is higher in deeper layer than near the surface. The water temperature near the ice edge is higher the freezing point -1.9 C. Blue and yellow lines in Fig. 11 show sea water temperatures versus time measured by SBE2 and SBE3 at the depths 6 m and 16 m. Temporal variations of the temperature in the open sea are larger than near the ice edge.

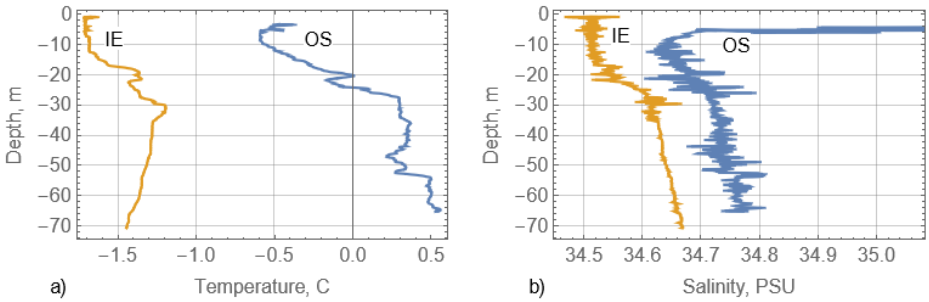

Figure 10. Temperature (a) and salinity (b) profiles measured near the ice edge (IE) and in the open sea (OS).

Polarsyssel was placed along the ice edge with rotating propellers until 14.40 UTC, March 9. Then, propellers were turned off until the end of the measurements. Figure 11b shows that sea water temperature recorded by SBE2 at 6 m depth started to rise around 15.00 UTC from -1.7 C reached -1.5 C during 30 min and then dropped below -1.7 C during next 30 min. Sensor SBE1 mounted below the ice at 45 cm depth also shows temperature rise, but smaller than SBE2. Temperature recorded by SBE1 was even higher SBE2 temperature around 16.00 UTC. The temperature rise was accompanied by downward motion of the water recorded by ADV (Fig. 12).

The ocean heat flux was calculated with standard formula $Q_w=\rho_{sw}c_{cw}\langle v'_z T'\rangle$ where ρ_{sw}=1028 kg/m^3 is the mean sea water density, c_{cw}=4.19 kJ/kg·K is the specific heat capacity of water, v'_z is the fluctuation of vertical water velocity, and T' is the fluctuation of the water temperature. Symbol $\langle\ \rangle$ means averaging over the specific interval of the measurements,

which was programmed to 1080 s within the burst interval of 1200 s. The fluctuations were calculated by the formulas $v'_z=v_z-\langle v_z\rangle$ and $T'=T-\langle T\rangle$, where v_z and T are the measured values of the water velocity and temperature. The heat fluxes are shown in Table 1. One can see that the fluxes were positive, i.e., directed upward, when ship propellers were working and pushing the ship to the ice. The heat flux turned to be negative when ship propellers were stopped. The large heat flux -99 W/m^2 calculated around 16.00 UTC, March 9, was accompanied by increasing of water temperature below the ice and downward water flux. Probably ship introduced significant changes in the water motion near the ice edge.

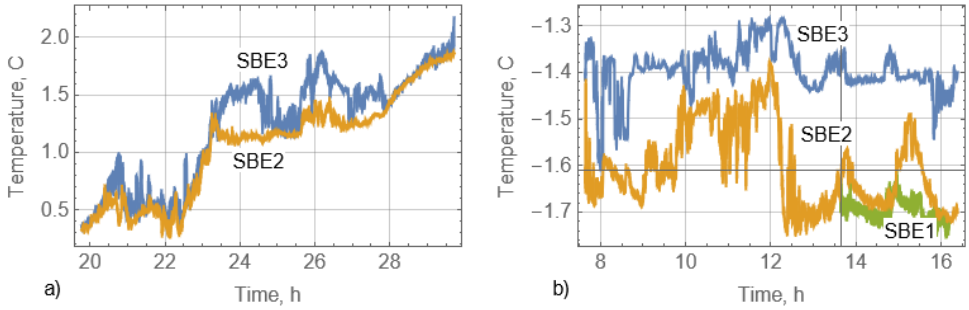

Figure 11. Sea water temperatures measured by SBE1, SBE2, and SBE3 in the open sea (a) and near ice edge (b). UTC time is accounted from 00.00 of March 8 (a) and March 9 (b).

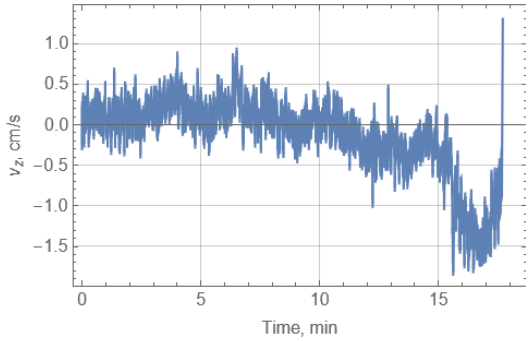

Figure 12. Vertical velocity of sea water versus time measured by ADV. The time calculation starts from 15.33 UTC, March 9.

Table 1. Heat fluxes below the ice calculated during 18 min measurements in each burst. UTC time on March 9 is pointed out.

Burst time, UTC	13.43	14.03	14.23	14.53	15.13	15.33
HF, W/m2	22.9	0.66	3.45	4.36	-5.41	-99.0

Sea ice properties

Photographs of vertical and horizontal thin sections in Fig. 13 show granular structure of ice near the ice edge with grain size of about 1 mm and smaller. Salinity of all specimens taken

from sea ice near the ship was around 5 ppt. The speed of p-waves measured with acoustic system Pulsar 2.2 (https://interpribor.com/pulsar-2.2) in the vertical and horizontal directions is shown in Table 2. The mean value of the horizontal speed was c_p=3.4 km/s.

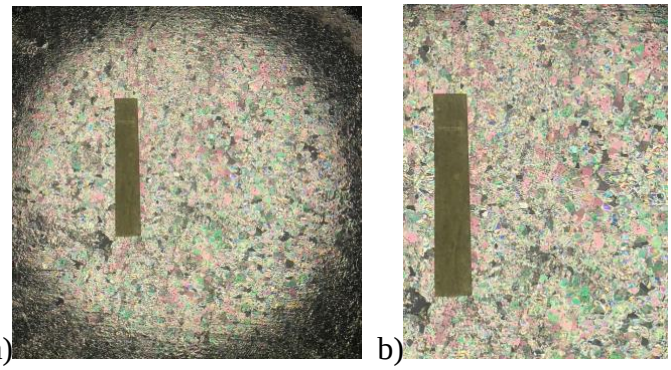

a) b)

Figure 13. Horizontal (a) and vertical (b) thin sections of sea ice. Yellow strips indicate 5 cm length.

Table 2. Speeds of p-waves in ice measured in the horizontal (H) and vertical (V) directions

Direction	H	H	H	H	V	V	V
c_p, km/s	3.5	2.6	4.1	3.7	3.9	2.2	3.7

The elastic modulus in the horizontal direction was calculated from the test with floating vibrating fixed-ends beam (Marchenko et al., 2020). The first eigen frequency ω_1 of floating fixed-ends beam is measured in the test. The beam is made in floating ice by sawing two parallel through ice cuts. Then, vertical vibrations of the beam are initiated by a shock and vertical accelerations of the beam are measured with the uniaxial accelerometer. The elastic modulus is calculated with the formula

$$E=12(\omega_1^2-\omega_b^2)(\rho_i h+m_{add})h^{-3}(a/2.365)^4,\ \omega_b^2=\rho_{sw}g(\rho_i h+m_{add})^{-1}, \quad (1)$$

where ρ_i=925 kg/m^3 is ice density, h is the beam thickness, ω_b is the frequency of buoyancy oscillations of the beam, m_{add} is the added mass per unit area of the beam surface, a is half length of the beam. The added mass is proportional to the amplitude of water pressure at the beam bottom, it is calculated with the formula (Grue, 2017; Marchenko et al., 2020)

$$m_{add}=4\rho_{sw}b\pi^{-2}\iint(\sin u\sin v)^2[u^2v^2((ub/a)^2+v^2)^{0.5}]^{-1}dudv, \quad (2)$$

where b is the half width of the beam.

In our test the beam shape was given by a=1m, b=0.1m, and h=0.17m. Vertical accelerations of the beam are shown versus time in Fig, 7b. The period of oscillations is estimated 0.021 s, and the first eigen frequency is ω_1=299 Hz. The calculated added mass is m_{add}=0.232 kg/m^3. The elastic modulus is calculated as E=0.47 GPa. The Poisson's ratio is calculated 0.49 with using of this value and c_p=3.4 km/s.

Flexural strength of ice beam was measured in 3-points bending tests. The load was applied to the middle of ice beams surface by hydraulic cylinder of 15 t power. The horizontal beams were taken from the ice and teste in natural orientation and flipped orientation. The dimensions of beam were 50 cm (length) and 5 cm (width and thickness). The ice salinity was of around 5 ppt, and the ice temperature was of around -5 C during the tests. Altogether 8 tests with naturally oriented beams, and 9 tests with flipped beams were performed. Tests results are shown in Fig. 14. The mean values of flexural strength are σ_{fs}=204 kPa (natural orientation), and σ_{fs}=170 kPa (flipped orientation).

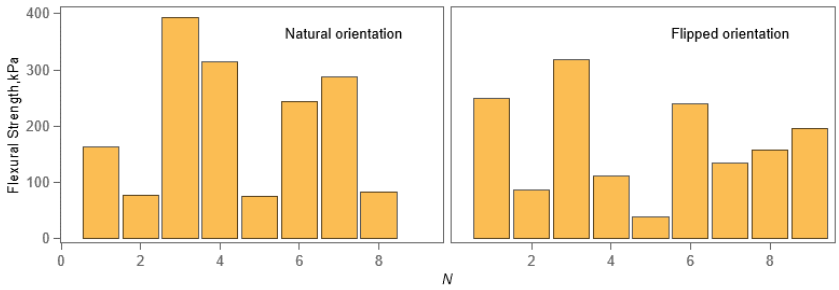

Figure 14. Flexural strength of ice beams with natural (a) and flipped (b) orientations.

4. DISCUSSION

Ice thickness h versus time t was estimated with the Stefan formula $h^2=2k\Delta Tt/(\rho_i L)$, where $\Delta T=T_f-T_a$, k=2.22W/m^{2}K, L=334 kJ/kg, and T_f =-1.9 C. Figure 15 shows the ice thickness calculated with the air temperature values shown in Fig. 1. One can see that the ice thickness is estimated larger in 1983, and the difference of the ice thicknesses in the beginning of March in 1983 and 2022 (t=150 days) is of about 20 cm. The actual ice thickness measured on March 8-9, 2022, was of around 20 cm near the ice edge. The reason for that can be the heat flux from ocean Q_w. The heat flux can be estimated with the formula (McPhee, 1992) $Q_w=\rho_{sw}c_{sw}\ u_*\Phi_T^{-1}(T_{sw}-T_f)$, where u_*=1cm/s is the turbulent velocity scale, and $\Phi_T\approx$200 is the Stanton number (Marchenko et al., 2016). According to Fig. 11b sea water temperature below the ice T_{sw} can be higher the freezing point on 0.2-0.5C. The equilibrium thickness of sea ice h_0 is calculated from the balance of heat fluxes from atmosphere and ocean as follows $h_0=k\Delta T/\ Q_w$. Assuming $T_{sw}-T_f$=0.4C we find h_0=0.026ΔT (m). Assuming ΔT=10C we estimate h_0=26 cm which is close to the observed ice thickness on March 8-9, 2022.

Squire (1984) doesn't inform on the date of the field works in 1983 when the ice thickness was of around 1 m. It is possible to assume colder sea water and smaller ocean heat flux at that time. Squire (1984) wrote that "In structure the ice was rather "mushy" and was polycrystalline". The ice salinity varied between 3 and 4 ppt, and ice temperature near the surface was -0.5 C and in deeper layers it was -1.8 C. It corresponds our observations. Therefore, further we compare characteristics of waves observed in 1983 and in 2022.

Line FGW in Fig. 16a is the dispersion curve of flexural gravity waves calculated with the formula $\omega^2=k(g+Dk^4)$, $D=Eh^3[12\rho_{sw}(1-\nu^2)]^{-1}$, where E=0.47 GPa, ν=0.5, and h=0.2m. Line

GW in Fig. 16a is the dispersion curve of gravity waves calculated with formula (8) and h=0. Points 1, 2, and 3 corresponds to local maxima of the spectrums in Fig. 5,6 with the frequencies 0.1 Hz (1), 0.155 Hz (2), and 0.4 Hz (3). One can see that the wave vectors and respectively wavelengths of the gravity waves with the frequencies 0.1 Hz and 0.155 Hz are similar the wave vectors and wavelengths of GRW with the same frequencies. The wavelengths of GW and FGW with the frequency 0.4 Hz are different. The length of GW (point 4 in Fig. 16a) is 9.7 m and the FGW length is 17 m.

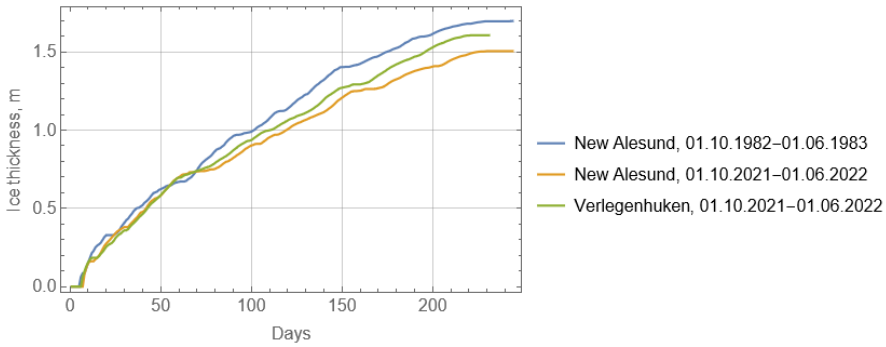

Figure 15. Ice thicknesses calculated by the degree days of the frost with Stefan formula.

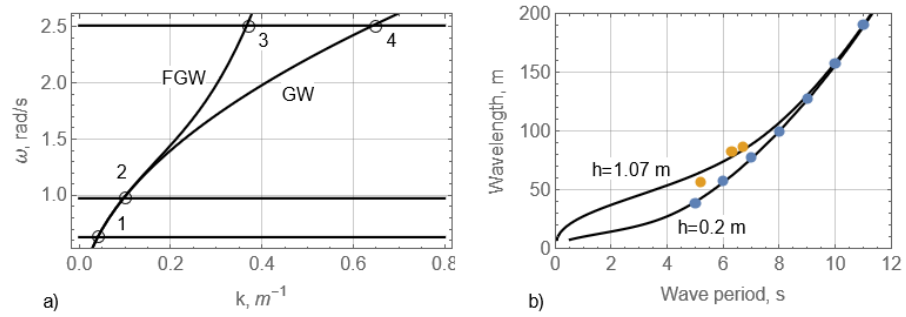

Figure 16. (a) Dispersion curves of gravity waves (GW) and flexural-gravity waves (FGW) in deep water. (b) Dispersion curves of FGW propagating below the ice with thickness 20 cm and 1.07 m.

The wavelength of FGW of 0.1 Hz frequency 156 m corresponds well to the shape of ice surface in Fig. 9a. Squire (1984) reported that waves with period 11 s had almost zero attenuation over 400 m distance. Figure 9 also confirms that such waves propagated below the ice without attenuations. Using cross-correlation analysis Squire (1984) reproduced dispersion curve of flexural gravity waves in Fig. 7. Simulation results are also shown in Fig. 7. Blue points in Fig. 16b are sitting on the dispersion curve in Fig. 7 from Squire (1984), and at the same time they correspond well to the dispersion curve FGW in Fig. 16a. Yellow points in Fig. 16b indicate simulation results shown in Fig. 7 of Squire (1984). They correspond better to the dispersion curve calculated with h=1.07 m in Fig. 16b. The condition of ice breakup by wave with length λ based on the elastic model of ice sheet is formulated in the form $\lambda=2\pi\{ahE/[2(1-\nu^2)\sigma_f]\}$. Dependencies $\lambda(a)$ calculated with elastic characteristics of sea ice measured in the Raudfjorden are shown in Fig. 17 for different ice thicknesses, E=0.5 GPa, ν=0.5, and σ_f=200 kPa. One can see that ocean swell with 10 s period practically can't

breakup thin ice with thickness 20 cm near ice edge if the wave amplitude is smaller 1 m. The ice can be broken by the swell in the regions with thicker ice located on some distance from the ice edge.

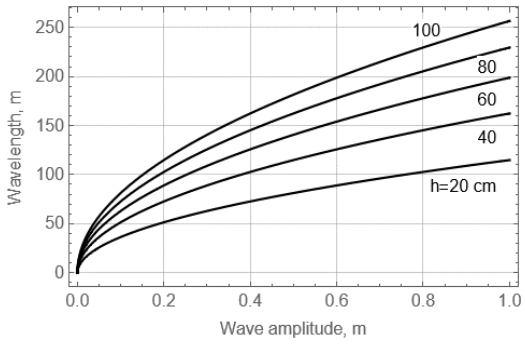

Figure 17. Wavelength versus wave amplitude.

5. CONCLUSIONS

Sea ice thickness in the Raudfjorden was smaller in 2022 in comparison to 1983 due to the influence of warm Atlantic waters on the ocean heat flux (Polyakov et al., 2017). The ice properties are characterized by granular structure, small elastic modulus of about 0.5 GPa and large Poisson's ratio 0.5 corresponding to incompressible material. Ocean swell with period 10 s penetrate below the ice without attenuation. Wind waves with period 2.5 s propagate below the ice with attenuation and can influence breakup of ice edge if their amplitude is big enough. The swell can breakup thicker ice located on some distance from the ice edge.

The work was supported by the Research Council of Norway through the IntPart project Arctic Offshore and Coastal Engineering in Changing Climate and SSG grant 311266.

REFERENCES

Grue, J., 2017. Ship generated mini-tsunami. J. Fluid. Mech., 816, 142-166.

McPhee, M.G. Turbulent heat flux in the upper ocean under sea ice. *J. Geoph. Res.* 1992, 97(C4), 5365-5379.

Marchenko, A., et al., 2016. Consolidation of Drifting Ice Rubble in the North-West Barents Sea. *Proceedings of the 23rd IAHR Symposium on Ice*, Ann Arbor, Michigan, USA.

Marchenko, A., 2018. Wave attenuation in marginal ice zone of Arctic pack ice to the North of Spitsbergen. *Proceedings of the 28th International Ocean and Polar Engineering Conference (ISOPE)*, 1642-1647.

Marchenko, A., et al., 2020. Elastic moduli of sea ice and lake ice calculated from in-situ and laboratory experiments. *Proceedings of the 22nd IAHR Symposium on Ice*, Trondheim, Norway.

Polyakov, I., et al., 2017. Greater role for Atlantic inflows on sea-ice loss in the Eurasian Basin of the Arctic Ocean. *Science* 356, 285–291.

Squire, V., 1984. A theoretical, laboratory and field study of ice coupled waves. *J. Geoph. Res*., 89 (NC5), 8069-8079.